YAC: A Code Using the Detailed Term Accounting Model for All-Z Elements

J. Yuan and G.A. Moses

August 2005

UWFDM-1276

Submitted to *Journal of Quantum Spectroscopy and Radiative Transfer*.

FUSION TECHNOLOGY INSTITUTE

UNIVERSITY OF WISCONSIN

MADISON WISCONSIN

YAC: A Code Using the Detailed Term Accounting Model for All-Z Elements

J. Yuan and G.A. Moses

Fusion Technology Institute
University of Wisconsin
1500 Engineering Drive
Madison, WI 53706

http://fti.neep.wisc.edu

August 2005

UWFDM-1276

Submitted to *Journal of Quantum Spectroscopy and Radiative Transfer*.

Abstract

We are developing an atomic code, YAC, for elements from low to high Z that explicitly include the detailed term structure. Detailed electron configurations are produced from a list of super-configurations. These detailed configurations are used as effective energy levels for population kinetics. Further, a list of all possible atomic processes such as photo-excitation (ionization), electron collision excitation (ionization) and autoionization is generated from these configurations and, except for the radiative transitions, these are calculated by using the configuration-average model. The spontaneous radiative transitions are calculated using the detailed term accounting model. The preliminary result for hard X-ray emission from a laser-irradiated plasma of U is presented.

1. Introduction

In spectral analysis of plasmas a fundamental tool is the collisional radiative model (CRM), which provides for the calculation of the population N_i of atomic level i. Solving the rate equations

$$\frac{dN_i}{dt} = -N_i \sum_j R_{ij} + \sum_j N_j R_{ji} ,$$

requires transition rates between all levels. Here R_{ij} is the rate coefficient for transition from level i to level j, which is dependent on the plasma condition. A rigorous method for calculating the populations requires the calculation of all transition rates between all the levels, construction of the transition matrix for all ion charges, and the solution of the large algebraic linear equation, and then construction of the spectrum from the level populations. For medium and heavy ions in hot dense plasmas of interest in laser fusion, applying this method is a challenging problem. The difficulties are several. One is that the number of levels and transitions involved is overwhelming. Although techniques have been developed to rapidly calculate large numbers of level-to-level radiative and collisional processes by using the factorization method [1], it is still not sufficient when numerous excited configurations and multiple charge ions are included. Even if the required transition rates are computed for all levels and ion stages, one encounters the difficulty of solving the resulting large linear equation system. Therefore, it remains necessary to make approximations to treat the numerous excited configurations.

One common approach is to use the whole configuration as an effective level instead of the detailed levels, and the rates for various atomic radiative and collisional processes connecting a pair of configurations are averaged statistically [2]. In this way, the number of levels involved in the rate equation is reduced dramatically, and the configuration-averaged rate coefficients can be evaluated without consideration of detailed angular coupling schemes. For example, the unresolved-transition-array (UTA) [3] method treats each configuration-to-configuration transition as a single broad unresolved structure represented by Gaussian profiles. The first and second moments of the transition energy weighted by the line strength are used as the average energy and the variance in the Gaussian profile. The UTA method has the advantage that it avoids the diagonalization of the Hamiltonian and thus the lengthy calculations for detailed line-by-line transitions. The method has been extensively used for the interpretation of both emission and absorption spectra which show broadband features. However, one also notes that individual lines corresponding to transitions between detailed levels exist as superpositions on the broadband structures. It has been shown that neglecting the resolved character of the transition arrays can lead to errors, especially for calculations of the Rosseland mean opacity that is sensitive to the gaps between lines [4]. For this reason, we calculate detailed transitions explicitly between initial and final configurations using the smoothness property of the reduced one-electron transition integral, a property that is also demonstrated for the integrals in the calculation of electron collision excitation. Using interpolation, a very large number of transitions can be rapidly calculated even for open L and M shells. In practice, we use 50,000 as the largest allowed number of line transitions between a pair of configurations allowed; the restriction required computer memory constraint. For larger transition numbers the relativistic single-electron single-transition UTA (RSSUTA) model [5] is applied. For atomic processes other than line transitions, the configuration-average approximation is used to calculate the rates for the CRM.

In this paper, we describe an atomic model which uses the detailed configurations as effective levels for the population equations but uses the detailed term accounting method for the line transitions. The relativistic formulae are adopted in order to apply to the high-Z elements. In Sec. 2.1, we outline the theory of the relativistic atomic structure, and discuss the radial wave functions in three different forms. In Sec. 2.2, we demonstrate the smoothness property of the one-electron transition integral, and because of this property and the use of interpolation, we are able to compute a larger number of line transitions. The various rate coefficients under the configuration-averaged approximation are discussed in Sec. 2.3. We summarize the formulae in a compact form and some results are compared with other theoretical calculations. The code structure is described in Sec. 3. The code is used as a postprocessor to a radiation hydrodynamics code to simulate the emission spectrum from laser-irradiated uranium plasmas. The preliminary results are given in Sec. 4.

2. Atomic model

2.1 Atomic structure

We adopt the relativistic atomic structure formalism to accurately treat atoms with Z > 30. As is standard in multi-configuration relativistic programs, the approximate atomic state functions are given by [6]

$$\Psi = \sum_{r=1}^{n_c} c_r \Phi_r , \tag{1}$$

where the mixing coefficients c_r are computed from the diagonalization of the Hamiltonian H, given by

$$H = \sum_{i=1}^{N} H_D(i) + \sum_{\substack{i,j \\ i<j}}^{N} \frac{1}{r_{ij}} , \tag{2}$$

where H_D(i) is the single-electron Dirac Hamiltonian due to its kinetic energy and nuclear potential. Φ_γ is the configuration state function which is built from products of one-electron Dirac spinors $u_{n\kappa m}$ and they are in turn solutions of the Dirac equation for a spherical central potential. The non-central part of the electron-electron electrostatic potential contributes as perturbations. The central potential is obtained by consistently solving with the Dirac equation,

$$\left[\frac{d}{dr} + \frac{\kappa}{r}\right] P_{n\kappa}(r) = \alpha \left[\varepsilon - V(r) + \frac{2}{\alpha^2}\right] Q_{n\kappa}(r) ,$$

$$\left[\frac{d}{dr} - \frac{\kappa}{r}\right] Q_{n\kappa}(r) = -\alpha \left[\varepsilon - V(r)\right] P_{n\kappa}(r) , \tag{3}$$

since the central potential $V(r)$ depends on the wave functions and is written as

$$V(r) = -\frac{Z}{r} + V_c(r) - \zeta \frac{3}{2}\left(\frac{3}{\pi}\rho(r)\right)^{1/3} , \tag{4}$$

where $V_c(r)$ is the direct term of the electron-electron potential energy and the third term represents the exchange term under Slater or Kohn-Sham approximation [7] when ζ equals to 2/3 or 1, respectively.

It is common that a single mean configuration with fractional occupation number is used to determine the self-consistent potential, such as in electron collision excitation calculations [8]. The mean configuration can be obtained by splitting the occupation of the active electrons approximately equally between initial and final shells – the method that is used here. The advantage is that all orbitals are automatically orthogonal since the potential is the same for all electrons including the continuum states, and this circumvents the non-convergence problems that occur in full multiconfiguration Dirac-Fock program such as GRASP.

For processes involving continuum states, one notes that it is much more time consuming to calculate the fully relativistic wave functions since the wave function is j dependent, which results in a factor of 4 (except for s orbitals) more radial functions than the non-relativistic waveform and thus an order of magnitude more radial integrals in calculations of the transition elements. The quasi-relativistic (QR) approach [8] keeps only the large component radial functions of Dirac waves. The potential is averaged over j value (κ=-1) so that the radial wave functions are independent of j. By making the substitution for $P_{n\kappa}$ with

$$F_{n\kappa} = a_P^{-1/2}(r) P_{n\kappa}(r), \tag{5}$$

into the Dirac equations and defining

$$a_P(r) = \alpha\left[\varepsilon - V(r) + \frac{2}{\alpha^2}\right],\ a_Q(r) = \alpha\left[\varepsilon - V(r)\right], \tag{6}$$

one obtains the equation for the large component [9]

$$\frac{d^2}{dr^2} F_{n\kappa}(r) + \xi(r) F_{n\kappa}(r) = 0, \tag{7}$$

where

$$\begin{aligned}\xi(r) = 2[\varepsilon - V(r)] - \frac{l(l+1)}{r^2} + \alpha^2[\varepsilon - V(r)]^2 + \frac{1}{r a_P(r)}\frac{dV(r)}{dr} \\ - \frac{3}{4a_P^2(r)}\left[\frac{dV(r)}{dr}\right]^2 + \frac{1}{2a_P(r)}\frac{d^2V(r)}{dr^2}\end{aligned}. \tag{8}$$

One can see that Eq. 7 is very similar to the non-relativistic Schrödinger equation with a more complicated additional term in the potential. In YAC, the QR radial function is actually solved with the solver for the Schrödinger equation with a slight change of the central potential. Both the Dirac equation and Schrödinger equation are solved on a hybrid mesh of the form [9],

$$x = ar + b\ln(r). \tag{9}$$

The advantage of using the hybrid mesh is that it incorporates the characters of both the logarithmic mesh, which is suitable for bound waves, and the linear mesh, which is appropriate for the continuum orbitals since they oscillate with large angular momentum l at large r. Three options, that is, fully relativistic, quasi-relativistic and non-relativistic, are provided for the bound and free radial wave functions. The free wave function is normalized such that the large component asymptotically oscillates as the Coulomb function at large r.

2.2 Line transition

The oscillator strength for the transition induced by a multipole radiation field operator of order L is [6]

$$f_{ij} = \frac{\pi c}{2L+1}\frac{1}{\omega^2}|< \Psi_i \| \hat{O}^L \| \Psi_j >|^2 \tag{10}$$

The transition matrix element is expressed in terms of configuration state function (CSF) matrix elements where the mixing coefficients, and the CSF matrix elements in turn are constructed from the single-electron transition integrals with angular coefficients. As in calculations for the collision strength of electron collisional excitation, the most time consuming part is to calculate the transition matrix elements for many transition energies. For electron collisional excitation, even more calculations are required for the many initial and final state angular momenta of the free electron. An efficient way for computing these radial integrals is to take advantage of the smoothness of the integrals and perform interpolation to rapidly obtain the integral at the needed transition energy. This approach allows us to calculate a large number of detailed line-by-line transition lines often resulting from open L and M shells. In YAC, up to 50,000 detailed transition lines are allowed, while for numbers larger than 50,000, the UTA method is used. Figure 1 displays the smoothly varying property for transition 3d-5f from initial configuration $1s^22s^22p^63s^23p^63d^{10}4s^24p^3$ for As-like uranium, which has 782 transition lines. The configuration interaction is included within the non-relativistic forms for the pair of initial and final configurations. In Fig. 2, we show the comparison for the oscillator strengths gf between YAC and GRASP for transition 2p-3d from an excited initial configuration $1s^22s^22p^63s^23p^63d^94p^2$. One can see that the oscillator strengths agree very well; however, differences arise for the transition energies. The difference for $2p_{1/2}$-$3d_{3/2}$ and $2p_{3/2}$-$3d_{3/2}$ is about 40eV and for $2p_{3/2}$-$3d_{5/2}$ is about 80eV, giving a relative error of 0.3%, which we suspect arises mainly from the central potential we choose.

2.3 Configuration-average approximation

The mixing coefficients, angular and radial integrals from the atomic structure calculations can be stored and used further for the detailed level-by-level collisional processes as it is done in the HULLAC code [10]. However, at the present stage of our code development, we use the configuration-average approximation for all other radiative and collisional processes. This approximation has been extensively used in the literature [11,12]. For completeness, here we present the formulation for calculations of various configuration-averaged collisional and radiative rates used in the code. The rates or cross sections can be written in a compact form consisting of an occupation number polynomial and a term only related to the active orbital wave functions as follows,

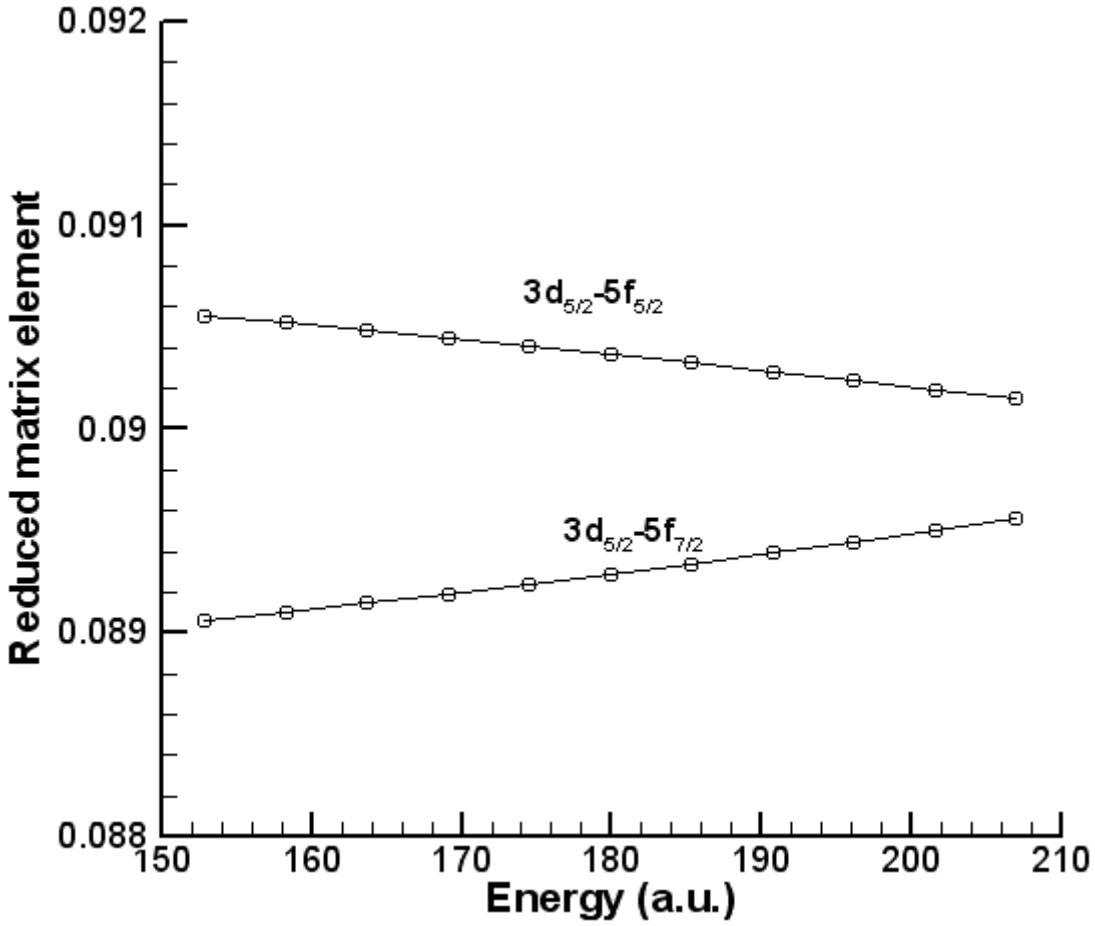

Fig. 1. Smoothly varying behavior for transition 3d-5f from initial configuration $1s^2 2s^2 2p^6 3s^2 3p^6 3d^{10} 4s^2 4p^3$ for As-like uranium.

$$Q_{C-C'} = q_\alpha^{n_\alpha}\left[1-\frac{q_\beta}{g_\beta}\right]^{n_\beta}\left[\frac{q_\gamma-\delta_{\alpha\gamma}}{g_\gamma-\delta_{\alpha\gamma}}\right]^{n_\gamma} Q_{\alpha\beta\gamma}\,, \tag{11}$$

where α, β and γ are the active orbitals and $n_{\alpha,,\beta,\gamma}$ are either 1 or 0 depending on the specific processes. $Q_{\alpha,\beta,\gamma}$ depends only on the orbital wave functions.

For electron collision excitation, one initial α and one final β electron are involved and thus $n_\alpha = n_\beta = 1$ and $n_\gamma = 0$. The "orbital" cross section is given by

$$Q(n_a l_a - n_\alpha l_\beta) = \frac{8\pi a_0^2}{(2l_\alpha+1)E}\sum_{ll'}\left[\sum_{\lambda=0}\frac{1}{2\lambda+1}\widetilde{D}_\lambda^2 + \sum_{\lambda=0}\frac{1}{2\lambda+1}\widetilde{E}_\lambda^2 + \sum_\lambda\sum_{\lambda'}(-1)^{\lambda+\lambda'+1}\begin{Bmatrix} l' & l & \lambda \\ l_\beta & l_\alpha & \lambda' \end{Bmatrix}\widetilde{D}_\lambda\widetilde{E}_{\lambda'}\right] \tag{12}$$

where the reduced direct and exchange Slater integrals are

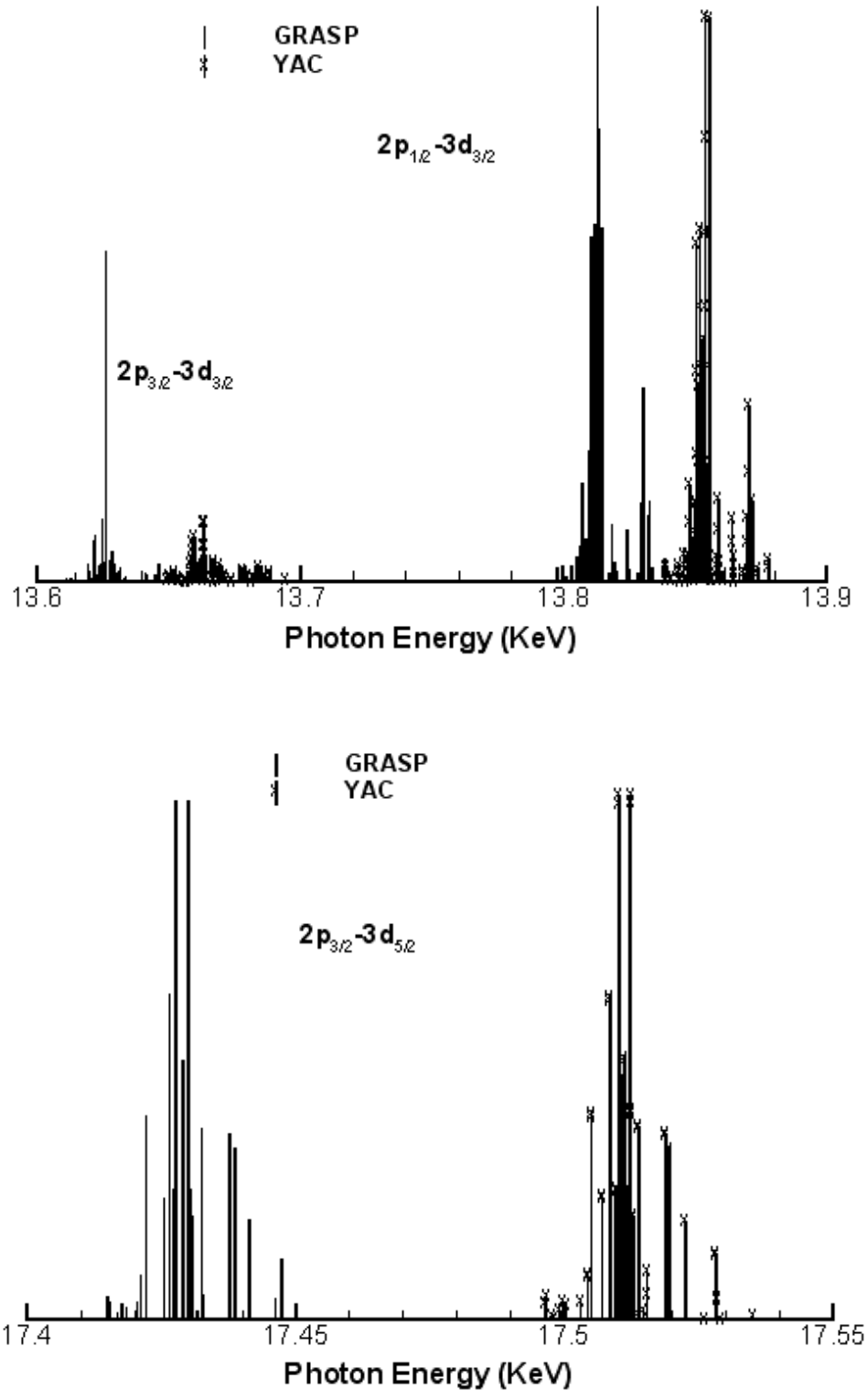

Fig. 2(a-b). Comparison for the oscillator strengths *gf* between the YAC code and the GRASP code for transition 2p-3d from an excited initial configuration $1s^2 2s^2 2p^6 3s^2 3p^6 3d^9 4p^2$ for Cu-like uranium.

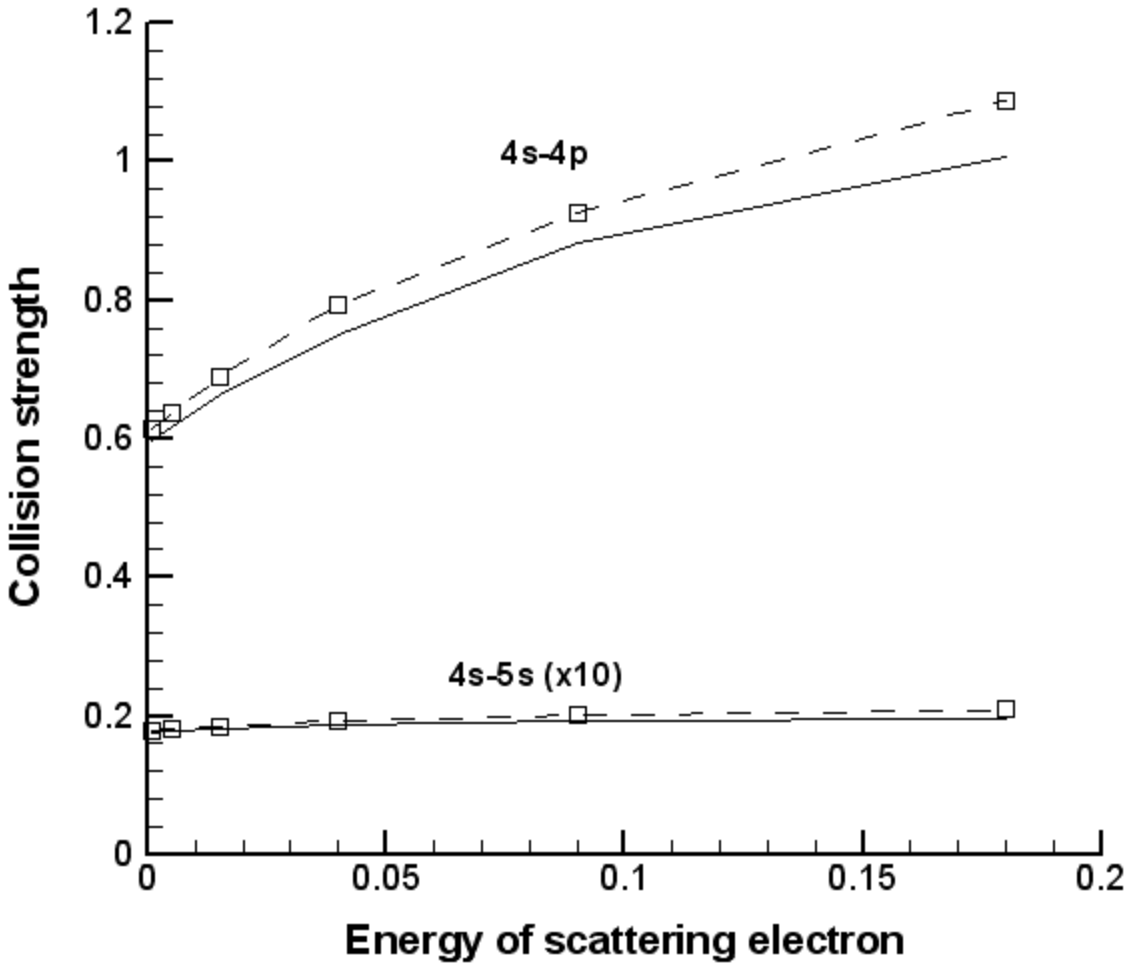

Fig. 3. Comparison of the collision strengths for excitations 4s-5s and 4s-4p with more sophisticated full-relativistic calculations for Cu-like uranium [13].

$$\begin{aligned} \widetilde{D}_\lambda &= < l_\alpha \| C \| l_\beta >< l \| C \| l' > D_\lambda \\ \widetilde{E}_\lambda &= < l_\alpha \| C \| l' >< l \| C \| l_\beta > E_\lambda \end{aligned}, \tag{13}$$

and D_λ and E_λ are direct and exchange Slater integrals, respectively. In YAC, electron collision excitation cross sections are calculated for all possible transitions between configurations, including excited and autoionizing configurations. The distorted waves are used for continuum states. The rate coefficients are obtained by weighting with a Maxwellian distribution at an appropriate electron temperature and its reverse process (collisional deexcitation) is calculated using the principle of detailed balance. In Fig. 3, we compare the collision strengths for excitations 4s-5s and 4s-4p with more sophisticated full-relativistic calculations for Cu-like uranium [13]. The discrepancy is within 10%, with some transitions better than 3%.

For electron collisional ionization, only one active electron is involved and thus $n_\alpha = 1$ and $n_\beta = n_\gamma = 0$. The corresponding "orbital" cross section is similar to the collisional excitation except that it needs to be integrated over the ionized electron energy and is given by

$$Q(n_a l_a) = \frac{8a_0^2}{(2l_\alpha+1)E}\int_0^{(\varepsilon-I)/2} d\varepsilon'' \sum_{ll'l''}\left[\sum_{\lambda=0}\frac{1}{2\lambda+1}\widetilde{D}_\lambda^2 + \sum_{\lambda=0}\frac{1}{2\lambda+1}\widetilde{E}_\lambda^2 + \sum_{\lambda}\sum_{\lambda'}(-1)^{\lambda+\lambda'+1}\begin{Bmatrix} l' & l & \lambda \\ l'' & l_\alpha & \lambda' \end{Bmatrix}\widetilde{D}_\lambda \widetilde{E}_{\lambda'}\right] \tag{14}$$

Autoionization occurs when an ion is excited into a level that lies above the next ion stage ionization limit. It is a two-electron process involving three active electrons, that is, one electron α goes to continuum while the other electron γ fills a lower orbital state β, and thus $n_\alpha = n_\beta = n_\gamma = 1$. The "orbital" rate for autoionization is given by

$$A(n_\alpha l_\alpha n_\gamma l_\gamma - n_\beta l_\beta) = \frac{2\pi}{\hbar}\sum_{l}\left[\sum_{\lambda=0}\frac{1}{2\lambda+1}\widetilde{D}_\lambda^2 + \sum_{\lambda=0}\frac{1}{2\lambda+1}\widetilde{E}_\lambda^2 + \sum_{\lambda}\sum_{\lambda'}(-1)^{\lambda+\lambda'+1}\begin{Bmatrix} l_\gamma & l & \lambda \\ l_\alpha & l_\beta & \lambda' \end{Bmatrix}\widetilde{D}_\lambda \widetilde{E}_{\lambda'}\right]. \tag{15}$$

In the code, all possible autoionizations to the ground state of the next ion stage are calculated, and rate coefficients for the reverse process (dielectronic recombination) are calculated from the principle of detailed balance.

The photoionization cross section for orbital α can be written as

$$\sigma_\alpha = \frac{\pi h e^2}{mc}\frac{df_\alpha}{d\varepsilon}, \tag{16}$$

where $\frac{df_\alpha}{d\varepsilon}$ is the density of oscillator strength, which is given by

$$\frac{df_\alpha}{d\varepsilon} = \frac{2m}{3\hbar\omega g_\alpha}|<\alpha \,||\, T \,||\, \varepsilon>|^2, \tag{17}$$

where $<\alpha \,||\, T \,||\, \varepsilon>$ is the transition matrix element from the initial bound orbital state α to the continuum orbital state ε. Radiative recombination is the reverse process of photoionization and it is calculated from the principle of detailed balance by integrating the cross section over an electron Maxwellian distribution at an appropriate temperature. All possible photoionizations from configurations of the target ion to configurations of the next higher ion stage are calculated in the code. The accuracy of the results is illustrated in Fig. 4 comparing with the analytic fits based on the Opacity Project [13].

The figure shows the partial photoionization cross sections of subshell electrons for Zn (Z=30) in ionization threshold units and one can see the agreement is very good.

3. YAC code description

The purpose of the code can be used to calculate the atomic structure and cross sections for radiative and collisional processes that are required in the rate equations for the simulations of non-LTE plasma spectra. The code is focused on medium and high Z elements with several open shells, but it can be applied to low Z elements as well. Sets of configurations for multiple ion stages to be included in the

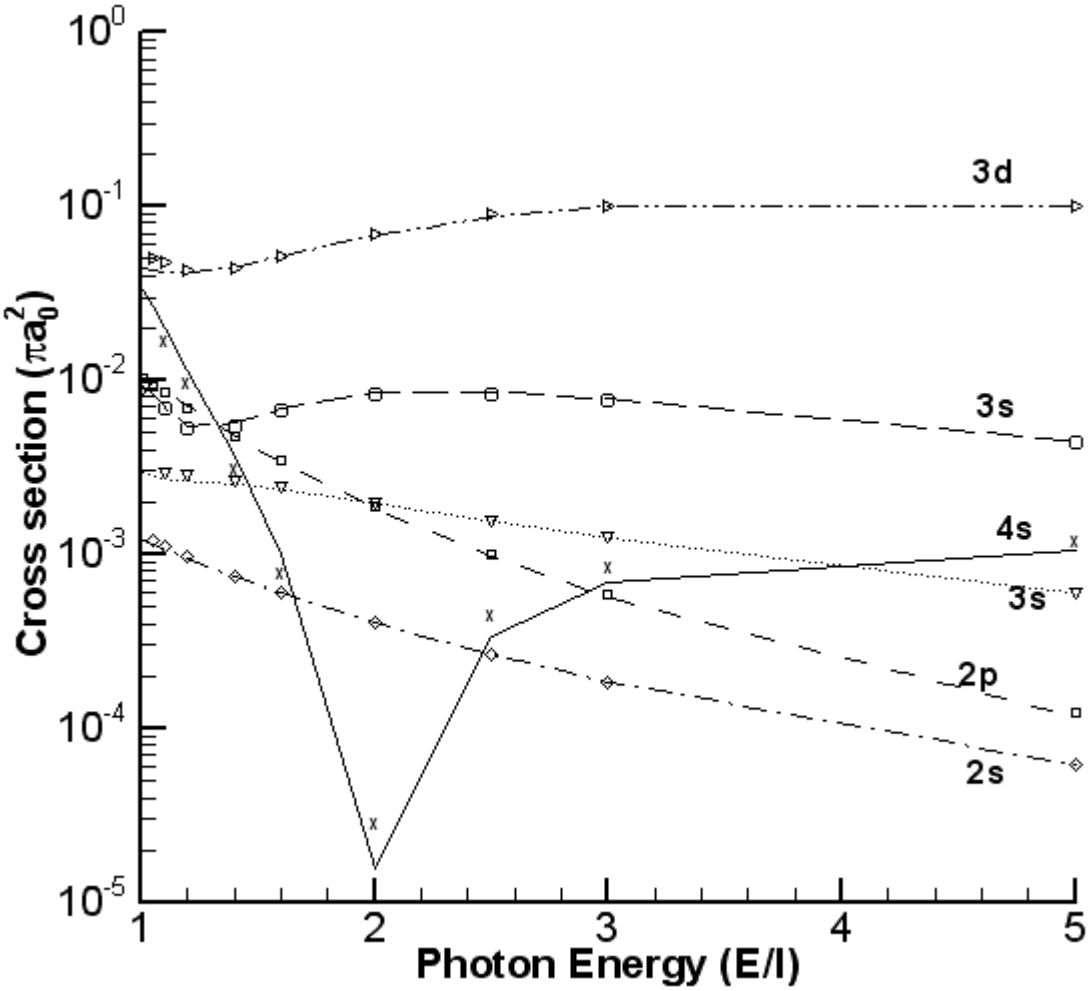

Fig. 4. Comparison of the partial photoionization cross sections of subshell electrons for Zn (Z=30) in ionization threshold units with the analytic fits based on the Opacity Project.

model are input by the user in the self-manifest XML format. YAC automatically generates all possible transition pairs for atomic processes such as photoexcitation and photoionization, electron collisional excitation and ionization, and autoionization. Atomic structure calculations start with the definition of the mean configuration from which the self-consistent-potential is obtained. The radial wave functions for both bound and free states are then computed from the same central potential using one of three methods, that is, by solving the fully relativistic Dirac equation, the non-relativistic Schrödinger equation or the quasi-relativistic approximation. The configuration state functions for all input configurations are pre-calculated and stored. The interaction configuration set is retrieved from the data store and merged to become the basis of the interaction configuration state functions. The Hamiltonian is diagonalized on the basis of these interaction state functions. The package developed by G. Gaigalas and Z. Rudzikas is used for angular jj-coupling [15].

Cross sections for processes other than photoexcitation, such as photoionization, collisional excitation and ionization, and autoionization, are calculated using the configuration-average approximation, as discussed in Sec. 2.3. For collisional excitation and ionization, a few points at impact electron

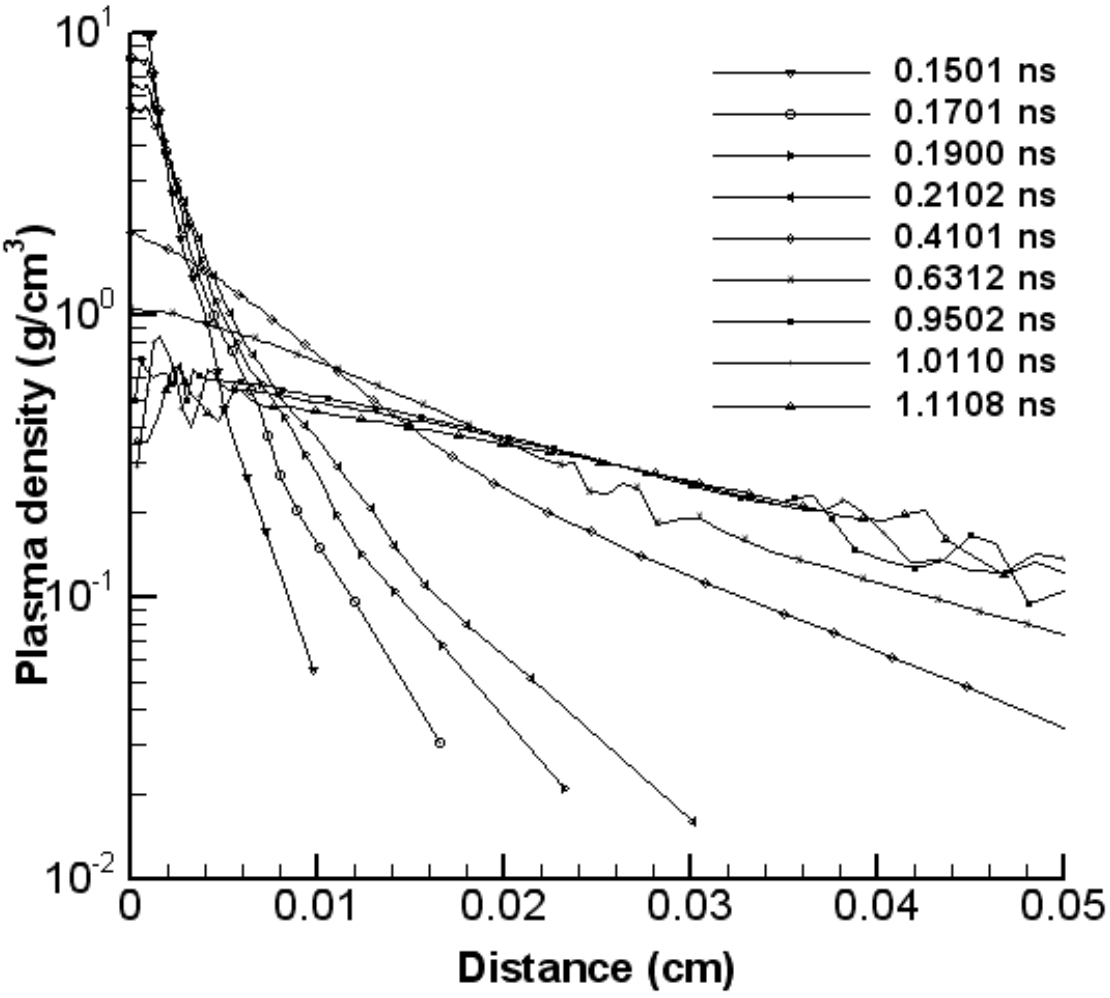

Fig. 5. The plasma density evolution versus the plasma expansion distance simulated by the 1D hydrodynamics code BUCKY.

energies spanning the range of transition energies are calculated for partial collision strengths and interpolation is used for the exact energy of each transition. This method reduces the computational time dramatically. The rates of these processes are obtained by integrating with a Maxwellian distribution at an appropriate temperature and the corresponding reverse processes are calculated by the principle of detailed balance.

The rate coefficients connecting the effective configuration levels are fed into the linear matrix solver for level populations, where currently a quasi-steady-state approximation is used. The size of the transition matrix is determined by the number of the configuration involved in the model. Having the configuration level population, the synthetic spectrum for either emission or absorption can be constructed with an appropriate line profile. A Java-based code for this is still under development [16]. Further, efforts are continuing to validate the code by comparing witht other theoretical calculation and experimental data.

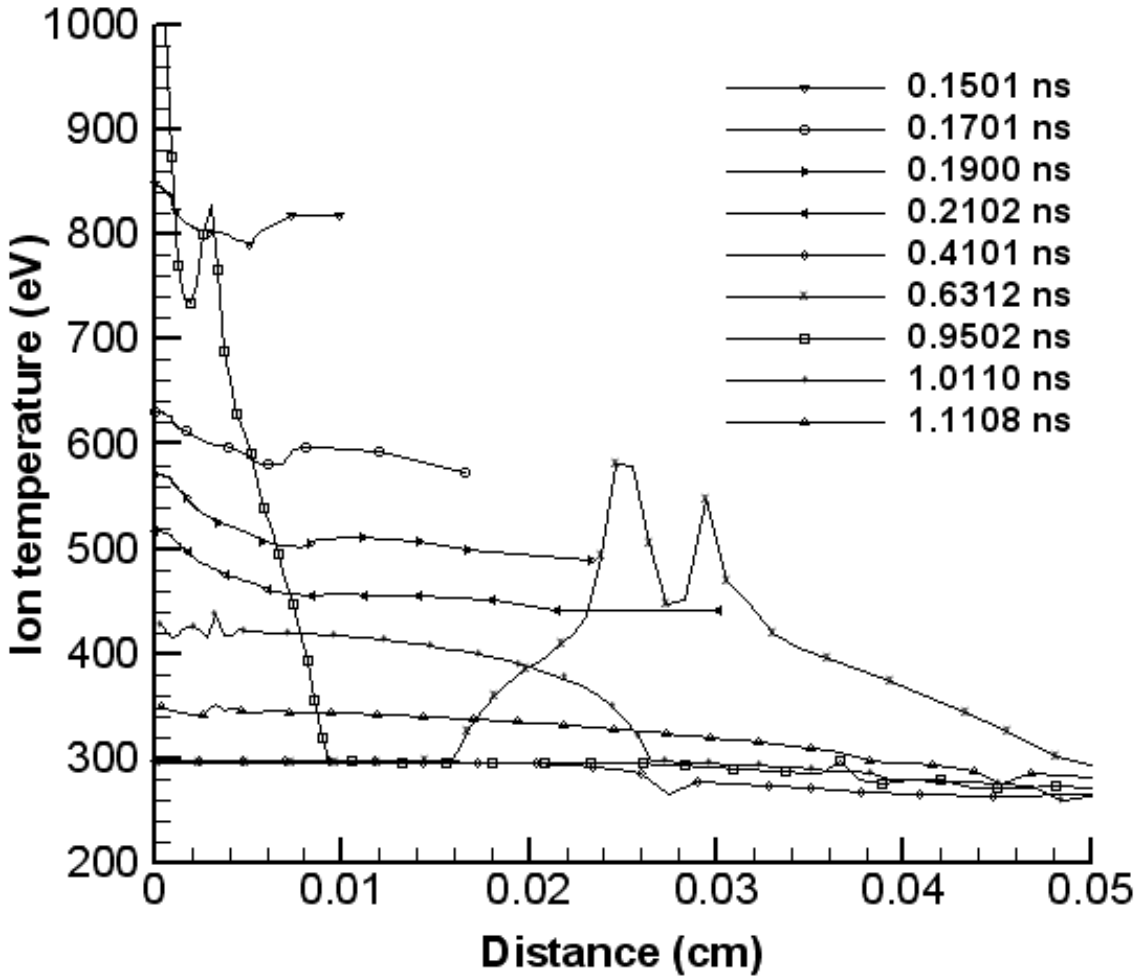

Fig. 6. The plasma temperature evolution versus the plasma expansion distance simulated by the 1D hydrodynamics code BUCKY.

4. Example simulations

As an example, we simulate the X-ray spectrum for a laser-irradiated U plasma [17]. The experiment was carried out at the OMEGA laser. The U foils with a thickness of 25 μm were irradiated by 24 beams, each with an energy of 500 J, and a pulse duration of 1 ns. Hard X-ray spectra were recorded by a transmission crystal survey spectrometer covering the 12-60 keV energy range with a resolving power of 100. The emission is of interest for the development of hard X-ray backlighters and hot electron diagnostics. The 1D hydrodynamic code BUCKY [18] in slab geometry was used to estimate the plasma condition.

Figures 5 and 6 show the plasma density and temperature evolution versus the plasma expansion distance, respectively. As we can see, the foil is heated rapidly and uniformly to about 820 eV at 0.15 ns, but the plasma density has a large gradient, dropping from the solid density at the slab center to 0.05 g/cm^3 at the expansion edge. With the continuing expansion, the radiation loss balances the laser deposition and thus the foil cools down to 300 eV at 0.4 ns. The gradient of the plasma density decreases because of the expansion. At 0.63 ns, the accumulated deposited laser energy at the outer

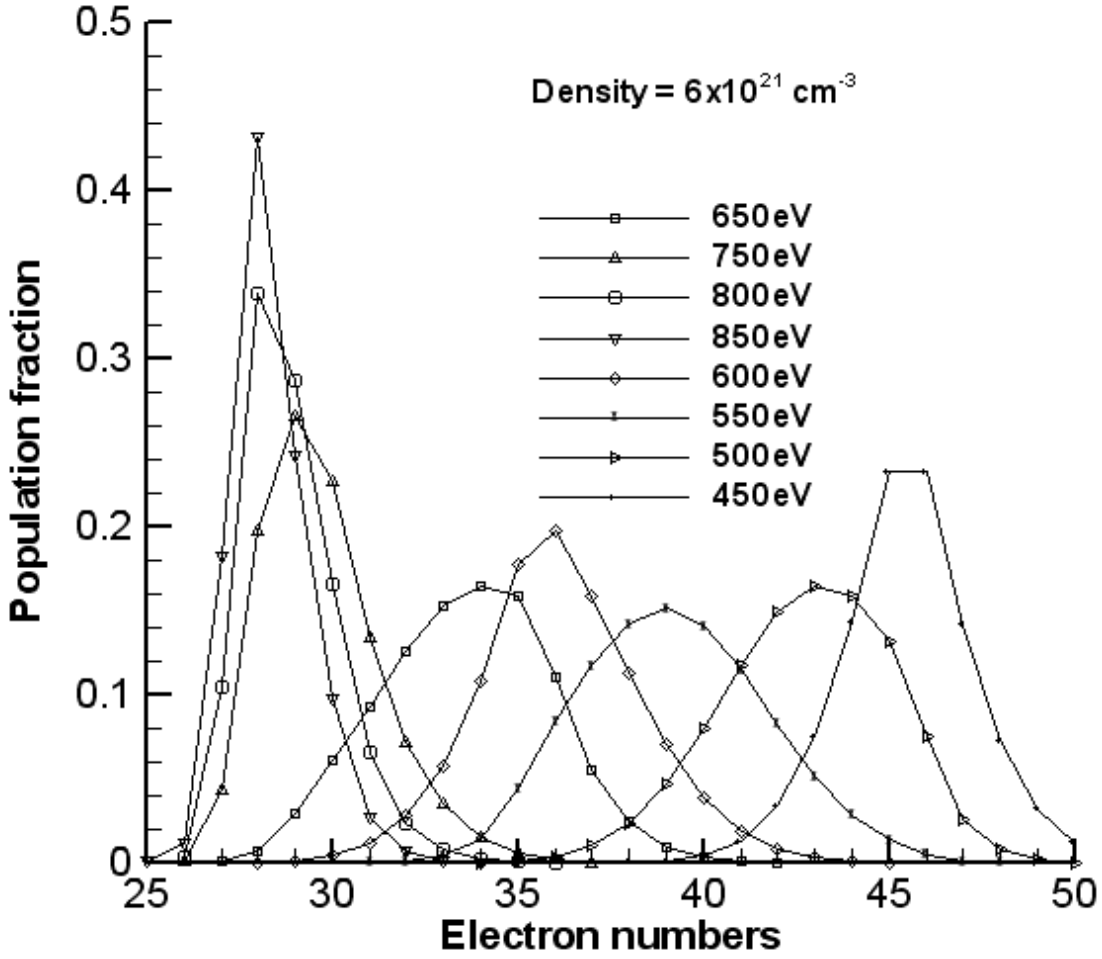

Fig. 7. Ionic distribution for different temperatures with a density of 6×10^{21}cm^{-3}.

region of the expanding plasma creates another thermal wave propagating towards the foil center. It drives high temperature above 1 keV at the foil center at 9.5 ns after which the foil cools when the laser turns off.

As a post-processor for analyzing the spectrum, we choose the plasma density at the middle of the expanding target, which is about 0.2~0.4 g/cm^3. At this density, we then estimate the plasma temperature by calculating the charge state population by solving the CRM equations for various temperatures from 450 eV to 850 eV, as shown in Fig. 7. We find that for temperatures much lower or higher than 650 eV, the dominant ions are shifted to the lower or higher ion stages which generate considerably lower or higher 2p-3d transition. Comparison with observations indicate that the 2p-3d are well-matched at a temperature of 650 eV. Therefore, we estimate that the plasma is of a temperature of 650 eV and a density of 6×10^{21}cm^{-3}. As we can see in Fig. 7, the ion stages span more than 10 ion species from Ni-like to Mo-like. For each ion, more than a hundred configurations are generated from a set of super-configurations. All the photoexcitation transitions for configurations having fewer than 4 open shells are computed in full relativistic configuration-interaction fashion.

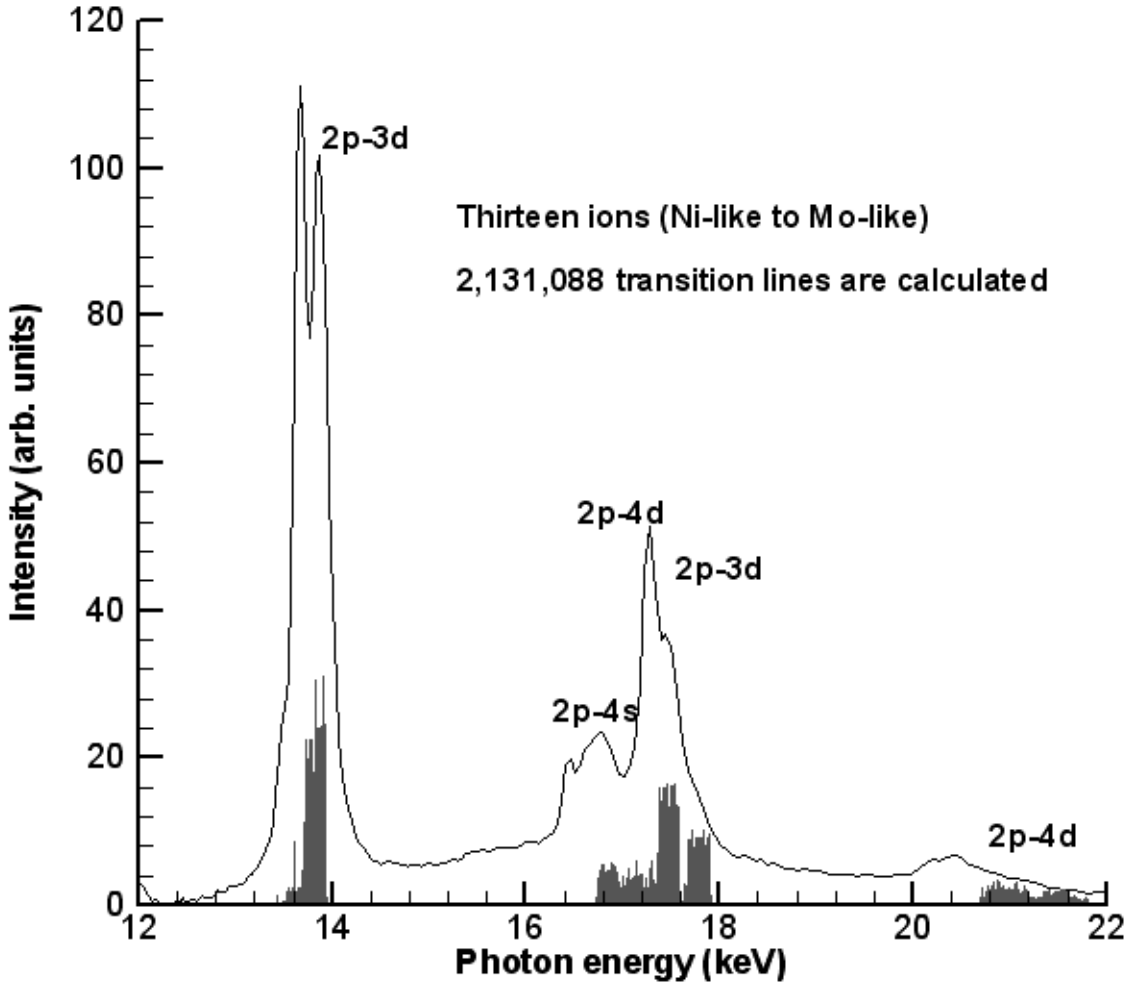

Fig. 8. Detailed line transition for thirteen ions from Ni-like to Mo-like uranium. Also shown is the experiment, shown as the solid line.

More than two million transition lines have been calculated for these thirteen ions and form band structures similar to experiment, as plotted in Fig. 8. The synthetic emission spectrum is shown in Fig. 9. The disagreements with the experiment can see in Fig. 9. Most notably: (1) the intensity ratio between the two sub-arrays within the strongest 2p-3d transition array (see Fig. 8 for reference), as also shown by HULLAC simulations [17]. This suggests that opacity effects and plasma density gradient effects may have a substantial role in forming the spectrum; (2) the predicted energy position for 2p-4d is higher than experimentally observed. We suspect this comes from the average-configuration potential, as illustrated previously; (3) the excited levels are not populated enough to produce the broadness of the emission structures when compared with experiment. These discrepancies indicate further improvements in the areas of level kinetics, atomic data and opacity effects are needed to compare with experiment for such a high Z element.

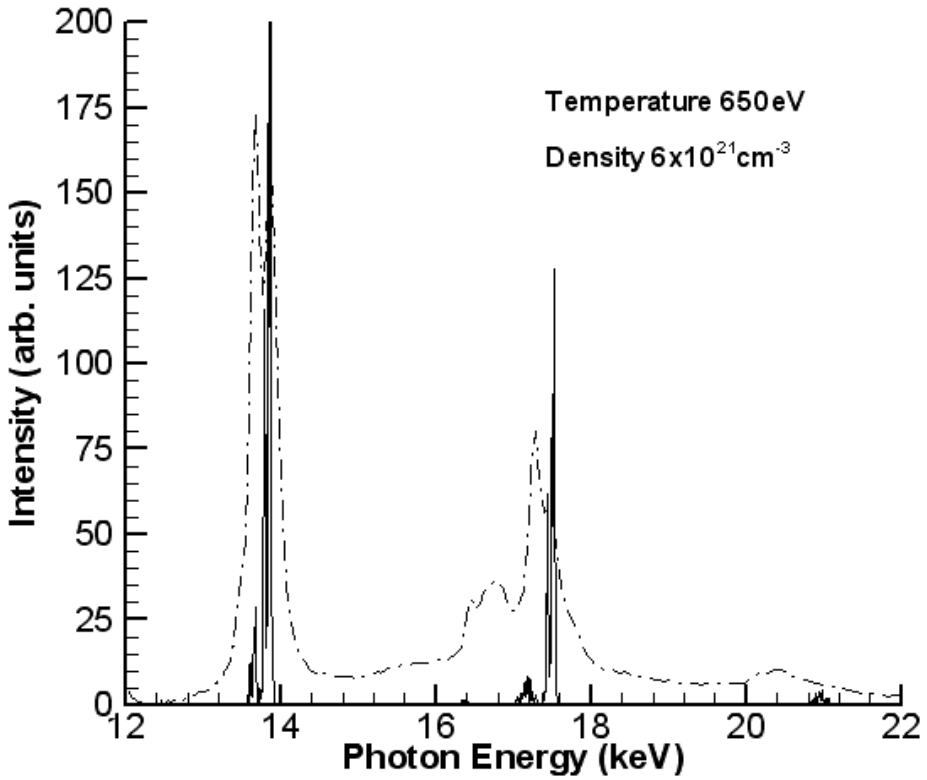

Fig. 9. Simulated emission spectrum of U plasma at temperature of 650 eV and a density of 6×10^{21}cm^{-3} compared with experiment, as shown as the dot-dashed line.

5. Conclusions and future work

We have described an atomic code, YAC, used to calculate the non-LTE plasma spectra using the detailed accounting method for line transitions. The configuration-average approximation is used for the other atomic process rates such as electron collisional excitation and ionization. These average-configurations are effective levels in the CRM population calculations. Good agreement is achieved when comparing with other theoretical models for atomic data, such as photoexcitation, photoionization, and electron collisional excitation.

An example of the code capability is given in a comparison with a laser-produced uranium plasma experiment and the 1D hydro code BUCKY is used to estimate the plasma conditions. More than two million transition lines have been calculated for thirteen ion stages for Ni-like to Mo-like U, including doubly-excited and triply-excited configurations. The transition lines form broad band-like structures similar to experiment. Disagreements between experiment and the synthetic spectra are noted, which suggest that further improvements on atomic data, population kinetics and plasma effects are needed.

Acknowledgements

This work is partially supported by the Naval Research Laboratory and Department of Energy. Further, we would like to thank J. R. Seely for the use of the experimental data.

References

[1] Bar-Shalom A., Klapisch M., and Oreg J., Phys. Rev. A 1988;38:1773.

[2] Abdallah Jr. J., Clark R.E.H., Kilcrease D.P., Csanak G., Fontes C.J., Proceedings of the 10th APS Topical Conference on Atomic Processes in Plasmas. AIP Proceedings 381, Jan. 1996; p. 131.

[3] Bauche-Arnoult C., Bauche J., Klapisch M., Phys. Rev. 1979;A20:2424.

[4] Iglesias C.A., Chen M.H., Sonnad V., Wilson B.G., JQSRT 2003;81:227-236.

[5] Yuan J., Haynes D.A., Peterson R.R., Moses G.A., JQSRT 2003;81:513-520.

[6] Dyall K.G., Grant I.P., Johnson C.T., Parpia F.A. and Plummer E.P., Com. Phys. Comm. 1989;55:425-456.

[7] Kohn W. and Sham L.J., Phys. Rev. 1965;A1133.

[8] Zhang H.L., Sampson D.H., and Mohanty A.K., Phys. Rev. 1989;40A:616.

[9] Hagelstein P. L. and Dalhed S., Phys. Rev. 1988;A37:1357.

[10] Bar-Shalom A., Klapisch M., Oreg J., JQSRT 2001;71:169-188.

[11] Peyrusse O., J. Phys. B: At. Mol. Opt. Phys. 1999;32:683-700.

[12] Bauche-Arnoult C., Bauche J., Luc-Kownig E. and Wyart J.F., Phys. Rev A 1989;39:1053.

[13] Verner D.A., Ferland G.J., Korista K.T., and Yakovlev D.G., Ap. J, 1996;465: 487.

[14] Zhang H.L., Sampson D.H. and Fonts C.J., Atomic Data and Nuclear Data Table, 1990;44:274.

[15] Gaigals G., Fritzsche S., IP. Grant, Com. Phys.Com 2001;139:263-278.

[16] Gui Z., Yuan J., Moses G.A., Bull. Am. Phys. Soc. Program of the 46th annual meeting of the division of plasma physics, Nov.15, 2004;49:114.

[17] Seely J.F., Doron R., Bar-Shalom A., Hudson L.T., C. Stoeckl, JQSRT 2003;81:421-429.

[18] MacFarlane J.J., Moses G.A., Peterson R.R., BUCKY-1, A 1-D Radiation Hydrodynamics Code for Simulating Inertial Confinement Fusion High Energy Density Plasmas, UWFDM-984, 1995.